THE JOURNAL OF PHYSICAL CHEMISTRY LETTERS
A JOURNAL OF THE AMERICAN CHEMICAL SOCIETY

pubs.acs.org/JPCL

Perspective

Quantum Dot Photocatalysts for Organic Transformations

Yucheng Yuan,[†] Na Jin,[†] Peter Saghy, Lacie Dube, Hua Zhu, and Ou Chen*

Cite This: *J. Phys. Chem. Lett.* 2021, 12, 7180–7193

Read Online

ACCESS | Metrics & More | Article Recommendations

ABSTRACT: Quantum dots (QDs) with tunable photo-optical properties and colloidal nature are ideal for a wide range of photocatalytic reactions. In particular, QD photocatalysts for organic transformations can provide new and effective synthetic routes to high value-added molecules under mild conditions. In this Perspective, we discuss the advances of employing QDs for visible-light-driven organic transformations categorized into net reductive reactions, net oxidative reactions, and redox neutral reactions. We then provide our outlook for potential future directions in the field: nanostructure engineering to improve charge separation efficiencies, ligand shell engineering to optimize overall catalyst performance, *in situ* comprehensive studies to delineate underlying reaction mechanisms, and laboratory automation with the assistance of modern computing techniques to revolutionize the reaction optimization process.

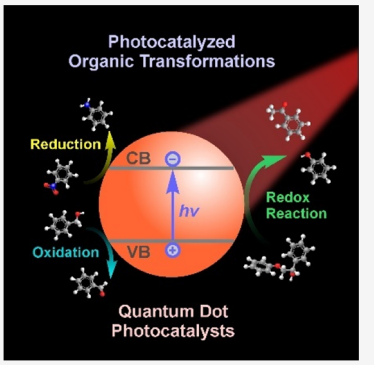

Photocatalytic reactions driven by visible light have drawn much attention for decades, because they allow us to make good use of sustainable solar energy with much reduced environmental concerns. Through absorption of light, photoexcited catalysts activate the substrates by charge or energy transfer, producing highly reactive radical intermediates that form certain products usually with high selectivity. In contrast to the traditional redox reactions, where high pressure and high temperature are often needed, photocatalytic reactions can occur using a small amount of photocatalysts under mild reaction conditions. As such, precious-metal-based photocatalysts, *e.g.*, tris(2,2′-bipyridine)ruthenium(II) ($Ru(bpy)_3^{2+}$) and *fac*-tris(2-phenylpyridine)iridium(III) ($Ir(ppy)_3$), have been extensively studied and fueled great achievements during the past several decades.[1−3] However, these precious-metal-based photocatalysts are not ideal for large-scale industrial applications because of their limited availability and high cost. Therefore, searching alternative photocatalysts that are composed of abundant materials and exhibit high catalytic efficiencies has been an active research topic in the past decades.[4−6] In this context, colloidal quantum dots (QDs) have emerged as one of the most promising candidates owing to their intrinsic advantages for photocatalysis. Upon light irradiation, an electron of a QD is excited to the conduction band (CB), leaving a positively charged hole in the initial valence band (VB). These photogenerated charge carriers can then migrate to the QD surface and separately catalyze net reductive reactions (using electrons) and net oxidative reactions (using holes) or collectively catalyze redox neutral reactions (Figure 1). QDs are in many ways ideal catalysts for organic transformations, highlighted by their tunable redox potential and unique catalyst−substrate interface. One can

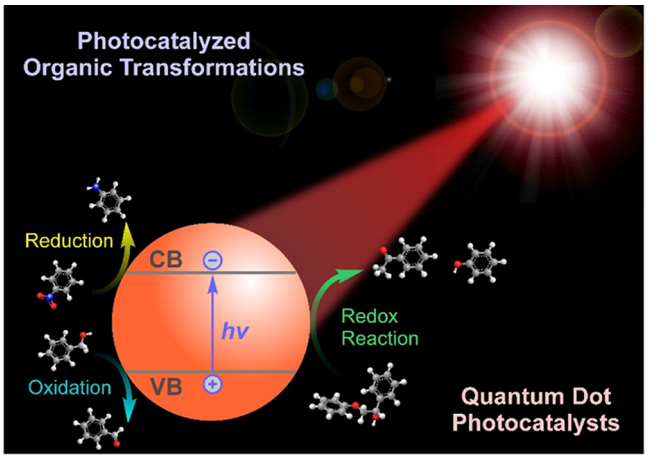

Figure 1. Schematic illustration of QD-photocatalyzed organic transformations.

QDs are in many ways ideal catalysts for organic transformations, highlighted by their tunable redox potential and unique catalyst−substrate interface.

Received: May 31, 2021
Accepted: July 19, 2021

https://doi.org/10.1021/acs.jpclett.1c01717
J. Phys. Chem. Lett. 2021, 12, 7180−7193

modulate the redox potential (mainly determined by the inorganic core through, *e.g.*, size and composition engineering) and catalyst−substrate interface (*via* surface atom control and ligand shell design) of QDs separately without reciprocal compromise.[7,8] Another advantage of QD catalysts for organic transformations in particular lies in their colloidal nature, which allows both sufficient interactions between the catalysts and substrates and the ease of catalyst removal from the reaction solution system, sharing the benefits of both homogeneous and heterogeneous catalysts. In addition, merits of QDs as photocatalysts also include large extinction coefficient, wide absorption spectral coverage, large catalytic surface area relative to volume, and high chemical and photostability.[9,10]

Because of the outstanding properties, scientists have been investigating the photocatalytic performance of QDs over decades, benefitting from the continuous achievements in the synthesis of such materials.[11−23] Studies on the utilization of QD photocatalysts for organic conversions have been more frequently reported in recent years, which provides new and effective synthetic routes to high value-added molecules and novel solutions to organic pollutant treatments under mild conditions.[24−27] In this Perspective, we summarize recent advances of QD-photocatalyzed organic reactions categorized into net reductive reactions, net oxidative reactions, and redox neutral reactions. We also provide useful information to enrich the field in terms of nanostructure designs for charge separation, ligand shell engineering for optimizing reaction efficiency, advanced *in situ* techniques to assist the exploration of underlying reaction mechanisms, and promising accelerated reaction optimization facilitated by modern computing technologies.

Studies on the utilization of QD photocatalysts for organic conversions have been more frequently reported in recent years, which provides new and effective synthetic routes to high value-added molecules and novel solutions to organic pollutant treatments under mild conditions.

Net Reductive Reactions. QD-catalyzed net reductive reactions utilizing photogenerated electrons have been commonly conducted under inert gas (*i.e.*, Ar or N_2) protection with sacrificial reductants (consuming holes) (Table 1). The pioneering works of employing QDs for net reductive organic reactions date back to the 1980s, the early development stage of QDs.[28,29] Owing to their highly negative reduction potentials, CdS and ZnS QDs were first employed by Yanagida to reduce aldehydes and Schiff bases to alcohols[28] and secondary amines,[29] respectively. Later, the reaction scope was expanded to reducing aliphatic or aromatic ketones,[30−33] and alkenes[31] to form aromatic alcohols or pinacols and alkanes, typically in the presence of triethylamine (TEA) as an electron donor. In the meantime, Yoneyama explored the electron transfer (ET) dynamics from different QDs, including PbS,[34,35] ZnS,[36] and CdS,[37] to methyl viologen. In addition, Yanagida also applied CdS and ZnS QDs to the dehalogenation of halogenated benzene derivatives to decrease the toxicity of organic halides.[38,39] Because the polyhalogenated compounds are electron-deficient molecules, their oxidation potentials are quite positive intrinsically. This results in a relatively slow oxidative degradation rate, leading to a favored reductive process of dehalogenation. In the recent past, ZnSe−CdS core−shell QDs were utilized for dehalogenation of aryl bromides and chlorides with various functional groups.[40] The formed type II bandgap alignment structure was beneficial for charge separation compared to pure CdS or ZnS QDs, and the reaction scope investigated in this report was expanded to the substrates with electron-withdrawing groups (*e.g.*, CN, CF_3, and COOMe).[40]

Table 1. Summary of QD-Photocatalyzed Net Reductive Reactions[a]

entry	catalyst (ligands)	cocatalyst	solvent(s)	atmosphere	hole scavenger	reaction type	light source	ref (year)
1	ZnS or CdS (S^{2-})	none	DMF	N_2	TEA	dehalogenation	500 W mercury lamp, >300 nm	38 and 39 (1998, 2001)
2	CdS or CdSe (aminothiol)	none	none		sodium formate	reduction of aromatic azides to amines	1 kW Hg−Xe lamp, ≥400 nm	41 (2004)
3	Rh-loaded CdS (silica)	Rh NCs	H_2O/*i*-PrOH	in SiO_2 shell	*i*-PrOH	reduction of NB to AZYB	7.3 mW cm^{-2} mercury lamp, 436 nm filter	42 (2007)
4	CdS (MEA)	none	*i*-PrOH	Ar	AF, *i*-PrOH	reduction of aromatic nitros to amines	3W LED, blue	43 (2014)
5	CdS (MPA)	none	H_2O/CH_3OH (80/20)	Ar	MPA, CH_3OH	reduction of NB to AN	7 mW laser, 405 nm	44 (2016)
6	ZnSe-CdS (stearate, TOP, OA, and ODA)	none	hexane	N_2	DIPEA	dehalogenation	2.45 W LEDs, 440−470 nm	40 (2017)
7	CdSe (oleate and TOP)	none	various	Ar	DIPEA	polymerization	10 W LED, 480 nm	45 (2018)
8	CdSe-CdS (mostly OAm)	none	toluene	Ar	4-fuorothiphenol	reduction of imines	3 W LED, green	46 (2018)
9	CdS (OPA)	none	NMP	Ar	DIPEA	cascade cycloaddition	36 W LED, blue	47 (2019)
10	CuInS−ZnS (MPO)	none	DMSO-d_6	Ar	TEA	removal of protecting groups	4.5 mW laser, 532 nm	48 (2020)

[a]DMF, *N*,*N*-dimethylformamide; AZYB, azoxybenzene; AF, ammonium formate; TOP, Tri-*n*-octyl phosphine; OA, oleic acid; ODA, octadecylamine; DIPEA, *N*,*N*-diisopropylethylamine; OAm, oleylamine; OPA, octyl phosphonate; NMP, *N*-methyl-2-pyrrolidone; MPO, 3-mercapto-1-propanol.

https://doi.org/10.1021/acs.jpclett.1c01717
J. Phys. Chem. Lett. 2021, 12, 7180−7193

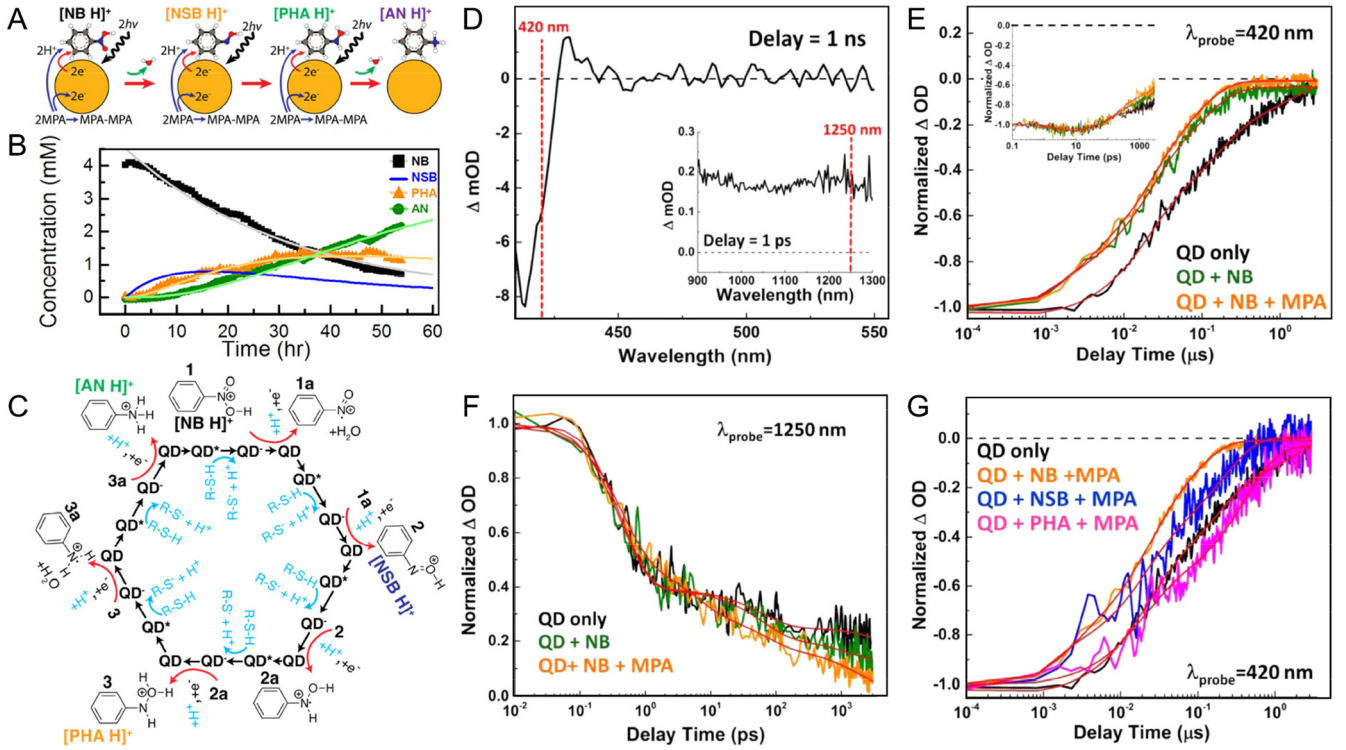

Figure 2. (A) QD photocatalyzing the reduction of protonated NB ($[NB H]^+$) to AN ($[AN H]^+$) through six sequential proton-coupled electron transfer steps, using MPA and MeOH as proton and terminal electron sources. (B) Time-dependent concentration of NB (initially 4 mM) and reduction products PHA and AN in the presence of 20 mM MPA and 4 nM CdS QDs. (C) Catalytic cycle for the six-electron, six-proton photoreduction of NB (**1**) to AN through NSB (**2**) and PHA (**3**) two-electron intermediates, all of which are partially protonated at pH 3.6. (D) Visible TA spectrum of 2 μM CdS QDs (no added NB or excess MPA) in 80:20 H_2O:MeOH, collected 1 ns after excitation at 390 nm. Inset: Near-infrared TA spectrum of the same sample of CdS QDs collected 1 ps after excitation at 390 nm. The red dotted lines mark two of the wavelengths at which the dynamics of the excited state of the QD were monitored, as shown in panels E and G. (E) Normalized kinetic traces extracted at 420 nm from the TA spectra of the 2 μM QDs (black), the QDs with 1000 equiv of NB (green), and the QDs with 1000 equiv of NB and 1000 equiv of MPA (orange). Inset: Normalized kinetic traces extracted at 420 nm from the TA spectra of the same samples but monitored on the ultrafast time scale (150 fs to 3 ns). (F) Normalized kinetic traces, monitored on the ultrafast time scale, extracted at 1250 nm from the TA spectra of the same samples as in panel E. (G) Normalized kinetic traces extracted at 420 nm from the TA spectra of the QDs (black), the QDs with 1000 equiv of NB and 1000 equiv of MPA (orange), the QDs with 1000 equiv of NSB and 1000 equiv of MPA (blue), and the QDs with 1000 equiv of PHA and 1000 equiv of MPA (pink). (A–G) Reproduced from ref 44. Copyright 2016 American Chemical Society.

Aromatic amines are one class of specifically targeted compounds in QD-based photoreduction reactions because of their broad utilizations in agricultural and pharmaceutical industries.[49] Successful examples of photocatalytic formations of aromatic amines include reductions of aromatic azides or aromatic nitro compounds catalyzed by CdS or CdSe QDs.[41,43,44] In conventional organic reactions, selectively reducing aromatic nitro compounds to amines, a six-electron, six-proton reductive process, without ceasing the reaction at intermediate stages and thus containing byproducts under mild reaction conditions, can be challenging.[50] In 2014, it was demonstrated that by using mercaptoethylamine hydrochloride (MEA) capped CdS QDs, aromatic nitro compounds of wide scope can be reduced efficiently to the corresponding aromatic amines, without producing the byproducts from the reduction of carbonyl and cyano functional groups on the aromatic rings.[43] To further understand the underlying mechanisms of QDs as photocatalysts, using nitrobenzene (NB) as a model substrate, Weiss's group later investigated the six-electron, six-photon photoreduction of NB to aniline (AN) catalyzed by CdS QDs *via* successive photoinitiated one-electron transfers in an acidic aqueous dispersion, which can be shown as a simple kinetic model of the three sequential reactions (Figure 2A).[44] Four-electron and six-electron photoproducts of phenylhydroxylamine (PHA) and AN were readily detected using gas chromatography–mass spectrometry (GC-MS), with the absence of two-electron intermediate nitrosobenzene (NSB).[44] The high product selectivity was attributed to the low reduction potential of NSB to PHA (+0.29 V), leading to irreversibly converting NSB intermediates to further reduced products, *i.e.*, PHA (Figure 2A,B). Governed by the limit of single-electron generation and utilization of the QD catalyst at a time under the applied photon flux condition, a photocatalytic cycle from NB to AN was proposed and outlined as shown in Figure 2C. When molecules are bound to the surface of nanoparticles, the nuclear magnetic resonance (NMR) signals for the protons close to the particles are broadened because of a prolonged rotational correlation time of the molecules. This signal-broadening effect makes NMR spectroscopy a powerful technique to differentiate and semiquantitatively determine the molecules adsorbed to the QD surface from free molecules in solution.[44] In this particular system, it was estimated that there were ~80 NB molecules absorbed on each QD by comparing the integration areas of the NMR signals from the molecules before and after mixing with QDs. Therefore, the catalytic cycle occurred through

https://doi.org/10.1021/acs.jpclett.1c01717
J. Phys. Chem. Lett. 2021, 12, 7180–7193

Table 2. Summary of QD-Photocatalyzed Net Oxidative Reactions[a]

entry	catalyst (lignds)	cocatalyst	solvent(s)	atmosphere	e^- scavenger	reaction type	light source	ref (year)
1	CdSe (DTO)	none	H_2O	air	O_2	carbon disulfide production	365 nm high-pressure mercury arc lamp	54 (2014)
2	CdS-TiO_2 (Brij-58)	none	acetonitrile	O_2	O_2	benzyl alcohol oxidation	>320 nm 300 W xenon lamp	62 (2015)
3	CdSe−ZnS (histidine)	none	H_2O	Ar	oxidant free condition	deoxyguanosine oxidation	420 nm halogen lamp	66 (2015)
4	CdSe (MPA)	Ni^{2+}	H_2O	Ar	oxidant free condition	benzyl alcohol oxidation	purple LEDs	60 (2017)
5	$CsPbI_3$ (oleate)	none	toluene and dichloromethane	air or Ar	O_2 or Bq	oxidative polymerization	solar simulator (LCS-100)	65 (2017)
6	CdS (oleate or BF_4)	none	highly alkaline aqueous solution	N_2	H_2O	plastic photoreforming	simulated solar light, AM 1.5G, 100 $mW{\cdot}cm^{-2}$	58 (2018)
7	CdS (PPA)	none	water−methanol	Ar	anthroquinone-2-sulfonate and methyl viologen	benzyl alcohol oxidation	405 nm 2.6 mW light	61 (2019)
8	CdSe-GR (MAA)	none	BTF	air	$K_2S_2O_8$	benzyl alcohol oxidation	>420 nm 300 W Xe arc lamp	63 (2019)
9	Bi-Bi_2WO_{6-x} (none)	none	H_2O	O_2	O_2	benzyl alcohol oxidation	420 nm 300W Xe arc lamp	64 (2019)
10	Mn-CdS/ZnS (silica)	deposited Pt NCs	H_2O	O_2	O_2	benzyl alcohol oxidation	405 nm 2.5 W LED	52 (2020)
11	$CsPbBr_3$ (DMOA-PS)	none	THF/toluene	air	O_2	stereoselective oxidative C−C coupling	435−445 nm blue LED	55 (2020)

[a]DTO, 1,1-dithiooxalate; Bq, 1,4-benzoquinone; PPA, phosphonopropionic acid; MAA, mercaptoacetic acid; BTF, benzotrifluoride; DMOA-PS, 3-(*N*,*N*-dimethyloctadecylammonio)propanesulfonate; THF, tetrahydrofuran.

"static" proton-coupled electron transfer reactions from QDs to pre-adsorbed molecules instead of a diffusion-controlled process.[44] In addition, transient absorption (TA) measurements were applied to monitor the transfer rates of electrons (monitored at 420 nm) and holes (monitored at 1250 nm) (Figure 2D−G). Results showed that each catalytic step occurred first by transferring a hole from the photoexcited QD to 3-mercaptopropionic acid (MPA, the hole scavenger) in 5.7 ps to form $QD^{\bullet-}$, which then can donate an electron to an adsorbed substrate molecule (*i.e.*, NB, NSB, and PHA) at the nanosecond time scale.[44] The rate constant for each electron transfer step was correlated to the thermodynamic driving force for the corresponding two-electron, two-proton reduction, which was consistent with the observation of concerted two-electron steps in the electrocatalysis of the same reaction.[44,51] More importantly, the rate constant implied that an electron transfer, rather than a proton transfer, was the rate-limiting step for each reduction process. Although this study provided meaningful insights on investigating the mechanism of QD-photocatalyzed reduction of NB, more research efforts are still needed to enrich the understanding of reaction mechanisms, especially for complicated multielectron, proton-coupled reactions.

Expanding the scope of QD-photocatalyzed organic transformations, photoexcited CdSe QDs were reported as efficient photocatalysts for radical-mediated polymerizations.[45] With reduction of the alkyl bromide initiator as the key step, different functional monomers were demonstrated to be able to drive the chain extension reactions.[45] Moreover, with improved material stability, CdSe−CdS core−shell QDs were proven to be stable and highly active photocatalysts for the proton-coupled electron transfer mediated reductions of imines to amines.[46] In addition, catalyzed by CdS QDs with a wide bandgap (2.42 eV), a broad range of CF_2-containing azaheterocycles were synthesized from dechlorogenation of ethyl chlorodifluoroacetate (ECDFA) and cascade cyclization with inactivated olefins.[47] The reactions were initiated by the reductive C−Cl bond cleavage of ECDFA through transferring one electron from a photoexcited CdS QD. The produced CF_2-containing azaheterocycles exhibited superior antiproliferative activity toward triple negative breast cancer and lung carcinoma cells, making them promising drugs for future cancer treatment.[47] Recently, it was also reported that CuInS−ZnS QDs can effectively photocatalyze the reductive deprotection of aryl sulfonyl-protected phenols.[48] Compared with $Ir(ppy)_3$, CuInS−ZnS QDs can absorb photons with energy as low as 730 nm (1.70 eV), and the interaction between substrate (*i.e.*, through carboxylic acid) and QDs can accelerate the deprotection rate of aryl sulfonyl-protected phenols.[48]

Net Oxidative Reactions. Unlike net reductive reactions, inert gas protection is not required in net oxidative reactions, as O_2 in the air sometimes promotes oxidation. To date, various kinds of QD-catalyzed oxidation reactions have been explored (Table 2), including oxidation of functional groups,[52,53] oxidative bond cleavage,[54] oxidative coupling,[55] *etc.*[56,57] In addition to producing useful molecules, attention has been particularly paid to oxidative environmental remediation, aiming to upgrade wastes into valuable chemicals.[58] Among all the reactions, alcohol oxidation represents one of the earliest and also the most widely studied net oxidative reactions catalyzed by QDs and is often used as a model reaction to evaluate the catalytic activity of QD-based photocatalysts. Traditional conversion of alcohols to carbonyl compounds often suffers from overoxidation and toxic oxidants, while the application of QDs with a finely adjusted redox potential as photocatalysts can potentially solve these problems. The earliest report of using QDs for alcohol oxidation dates back to 2008, when Palmisano and co-workers employed rutile TiO_2 nanocrystals (NCs) for selective photo-

https://doi.org/10.1021/acs.jpclett.1c01717
J. Phys. Chem. Lett. 2021, 12, 7180−7193

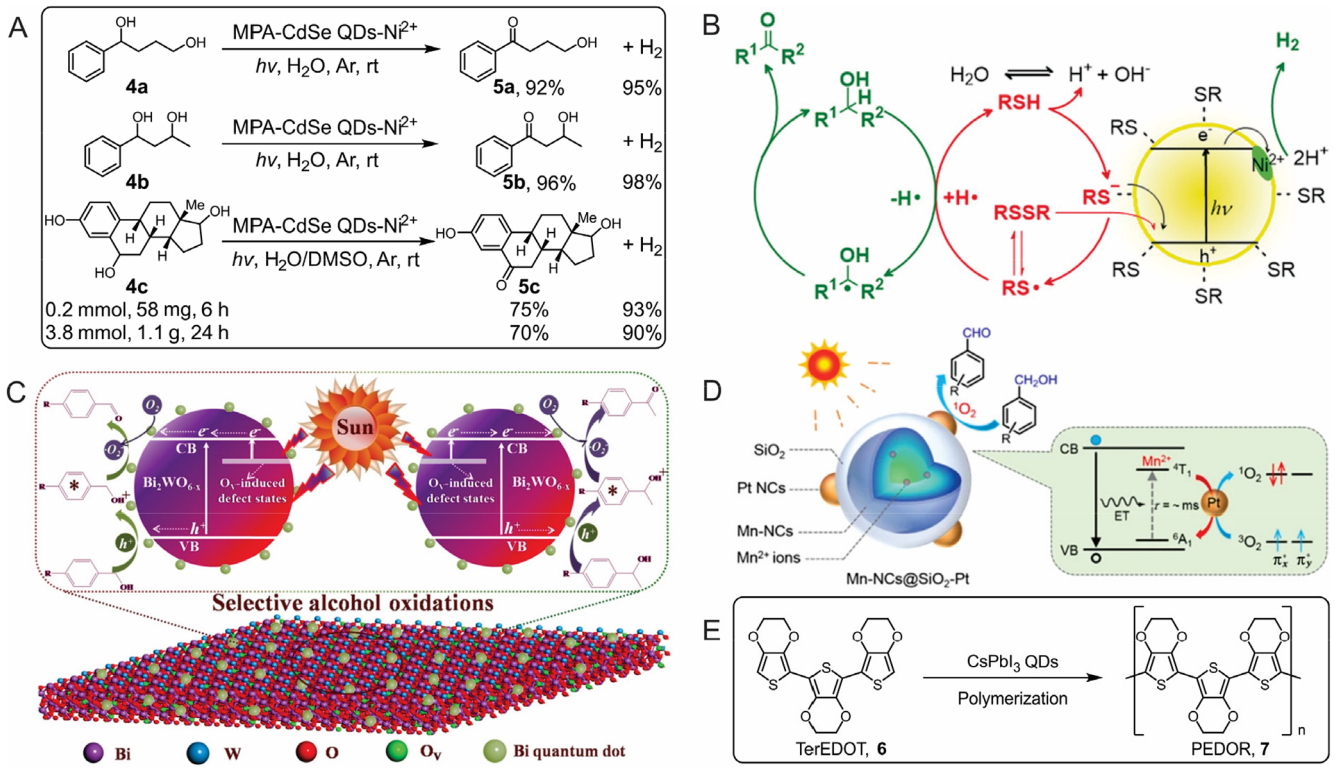

Figure 3. (A) Site-selective photo-oxidation of polyhydroxy alcohols to aldehydes/ketones catalyzed by CdSe QDs. Reproduced with permission from ref 60. Copyright 2017 Wiley-VCH GmbH. (B) Benzyl alcohol oxidation through a radical relay process using CdSe QDs. Reproduced with permission from ref 60. Copyright 2017 Wiley-VCH GmbH. (C) Bi_2WO_{6-x} nanosheets with tunable Bi QDs and oxygen vacancy heterostructure, and the mechanism for facilitated charge transfer. Reproduced with permission from ref 64. Copyright 2019 Elsevier B.V. (D) Mn-NCs@SiO_2-Pt heterostructures and the mechanism for facilitated QD charge transfer. Reproduced with permission from ref 52. Copyright 2020 Tsinghua University Press and Springer-Verlag GmbH Germany, part of Springer Nature 2020. (E) $CsPbI_3$ perovskite QDs catalyzed polymerization of TerEDOT. Reproduced from ref 65. Copyright 2017 American Chemical Society.

oxidation of benzylic alcohols to aldehydes in water.[59] Inspired by this study, different QD-based catalytic systems were explored to understand the alcohol oxidation mechanism in a wide range of alcohols with incredibly high selectivity. For example, site-selective oxidation of polyhydroxy alcohols to aldehydes/ketones has been achieved using MPA-capped CdSe QDs (MPA-CdSe QDs) (Figure 3A).[60] The thiyl radical was generated from transferring an electron to the MPA ligand, which played an essential role in extracting the H atom from the C−H bond of the alcohol through a radical relay process (Figure 3B).[60] CdS QDs were also reported to convert benzyl alcohol to benzaldehyde with 99% selectivity. More interestingly, through tuning the number of Cd^0 on the surface of the CdS QDs, one can direct the reaction to produce either benzaldehyde (less Cd^0) or C−C coupled products (more Cd^0).[61] In addition to using pure QDs, different design strategies have been explored to improve catalytic efficiencies, among which QD-based hybrid materials present one of the most promising means. For instance, an interconnected network of CdS QDs and TiO_2 NCs was reported by Armatas and colleagues.[62] This hybrid system with a narrower bandgap (comparing to the sole TiO_2 NCs) improved catalytic efficiency from 38% to 99% under visible light illumination.[62] Xiao *et al.* developed a three-dimensional, layer-by-layer assembled CdSe QDs−graphene nanosheet (CdSe-GR) heterostructure through electrostatic interactions.[63] The efficiency of the CdSe-GR for selectively oxidizing aromatic alcohols to the corresponding aldehydes far exceeds that of pure CdSe QDs.[63] The improvement was ascribed to the prolonged excited-state lifetime due to electron shuttling from CB of CdSe QDs to graphene nanosheets, as well as enlarged catalytic surface area originating from graphene nanosheet intercalation.[63] The design of metal doping and/or nonmetal vacancy has also been explored to improve the catalytic performance. As one example, Bi_2WO_{6-x} nanosheets with tunable amounts of Bi QDs and oxygen vacancies were synthesized for selective aromatic alcohol oxidation.[64] The greatly enhanced activity of this photocatalyst was mainly attributed to the introduction of both Bi QDs and oxygen vacancies (Figure 3C), which resulted in the formation of an intrabandgap defect state that was responsible for the enhanced light-harvesting ability and charge separation efficiency.[64] In another example, silica-coated Mn-doped CdS/ZnS QDs decorated with Pt NCs (Mn-NCs@SiO_2-Pt) were fabricated to lengthen the excited-state lifetime.[52] Owing to the long-lived excited state of Mn dopants (several milliseconds), the energy transfer between Mn-doped CdS/ZnS QDs and molecular oxygen was facilitated with the assistance of the deposition of Pt NCs on the Mn-NC@SiO_2 surface (Figure 3D). The resulting Mn-NCs@SiO_2-Pt composite exhibited excellent catalytic activity and selectivity for the oxidation of primary benzylic alcohols to aldehydes through an $^1O_2$ engaged oxidation process.[52] It is noteworthy that, although the role of hybrid QD-heterostructures in facilitating charge separation has been widely studied in different systems, whether introducing dopants/vacancies to

https://doi.org/10.1021/acs.jpclett.1c01717
J. Phys. Chem. Lett. 2021, 12, 7180−7193

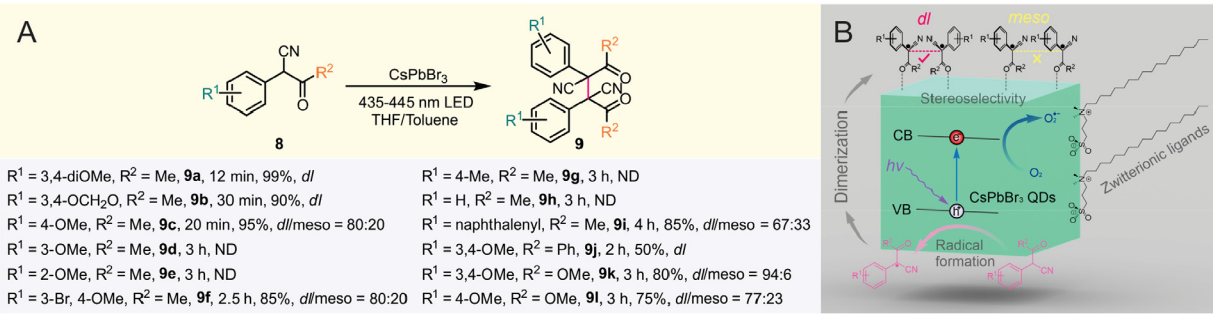

Figure 4. (A) Reaction scope and (B) proposed reaction scheme of the stereoselective dimerization of α-aryl ketonitriles photocatalyzed by ZW-$CsPbBr_3$ perovskite QDs. (A and B) Reproduced with permission from ref 55. Copyright 2020 Wiley-VCH GmbH.

the QD-based catalysts facilitates or inhibits catalytic reactions remains controversial.[10] The intrinsic complexities of dopants/vacancies (*e.g.*, dopant/vacancy type, concentration, and geometrical location) complicate the interaction between the QD-host and the dopants/vacancies, often making it difficult to draw a decisive conclusion.

While we elaborate on alcohol oxidation, there are a variety of other photo-oxidative reactions catalyzed by QDs, such as oxidation of cyclohexane,[67] deoxyguanosine,[66] and gas-phase *o*-oxylene,[68] epoxide ring-opening reactions,[69] dithiooxalate to CS_2 conversion,[54] and coupling reactions.[70] In this section, we focus on oxidative coupling because of its significance in synthetic chemistry, pharmaceutical design, organic materials and polymer development, *etc.*[71] In 2017, Chen *et al.* reported the application of $CsPbI_3$ perovskite QDs as photocatalysts for an oxidative polymerization.[65] In this reaction, 2,2′,5′,2″-ter-3,4-ethylenedioxythiophene (TerEDOT) monomer was specifically chosen instead of the commonly used 3,4-ethylenedioxythiophene (EDOT). This is because the oxidation potential of the TerEDOT measured by cyclic voltammetry (CV) lies above the VB of $CsPbI_3$ perovskite QDs, which enables charge transfer between the substrate and the QDs. Upon oxidation by $CsPbI_3$ QDs, the TerEDOT monomer forms a positively charged intermediate, which can further go through a self-polymerization process to form poly(3,4-ethylenedioxythiophene) (PEDOT). Interestingly, the photocatalytic polymerization naturally produced the polymer-encapsulated $CsPbI_3$ QDs, providing an energy-efficient *in situ* method for fabricating QD−polymer conjugates, which can be potentially utilized in optoelectronics.[65]

Recently, our group reported a work of stereoselective C−C coupling reactions of α-aryl ketonitriles (selectivity of >99%) using zwitterionic ligand-capped $CsPbBr_3$ (ZW-$CsPbBr_3$) perovskite QDs (Figure 4).[55] We found that the zwitterionic ligand coating can not only improve the stability of $CsPbBr_3$ QDs for catalyst recycling and reuse but also increase the photocatalytic reaction rate by ∼3.5 times. This enhanced reactivity can be attributed to a reduced density of surface ligand coverage and thus an increased accessibility of the substrates to the particle surface (catalytic sites), lowering the kinetic barrier of the reaction.[55] A reaction scope study revealed that electron-donating groups or large conjugated π systems were necessary for the efficient C−C oxidative coupling reactions (Figure 4A).[55] All the products exhibited a stereoselectivity of *dl*-isomers, which are hardly accessible using other oxidants or catalysts. Furthermore, DFT calculations of the bond dissociation energies explained the generation of dimers, which are energetically favored rather than benzo[*b*]furans, another commonly formed type of products under oxidative conditions. The substrate radical intermediate and superoxide trapped by 5,5-dimethyl-pyrroline *N*-oxide, a radical scavenger, were detected by electron paramagnetic resonance measurements, indicating that the reaction underwent a free-radical-mediated reaction pathway.[55] The observed stereoselectivity of *dl*-isomers was induced by steric hindrance effect between neighboring substrate molecules assembled on the perovskite QD surface during the C−C bond formation process (Figure 4B).[55] Our study demonstrates that QDs with optimized ligand passivation hold the potential of acting as efficient photocatalysts for organic transformations with enhanced product yield and selectivity.

Increased environmental concerns have attracted scientists' attention toward catalytic degradation of wastes. QD photocatalysts represent one promising candidate for degradation of various organic pollutants, including organic dyes;[72] pharmaceuticals (especially antibiotics); pesticides;[73] and other industrial wastes, such as toluene.[74] Nonmetal-based materials, such as graphene QDs and carbon QDs, are of particular interest in photodegradation of wastes because of their environmental friendliness. In many cases, these organic pollutants can be directly converted to nontoxic CO_2 and H_2O. Researchers also seek to upcycle these wastes into valuable chemicals. For example, plastic photoreforming and upcycling reactions with the potential of using plastic waste as the feedstock for fuel production (such as H_2 generation) attracted much attention in recent years.[58] A pretreatment of plastics using highly concentrated alkaline solutions was commonly applied to first break down plastics to release monomers or oligomers, which can be subsequently transformed to smaller molecules through photo-oxidation reactions catalyzed by QDs.[58,75] The Reisner group reported that high plastic conversion rates can be achieved for different types of polymers (*i.e.*, polylactic acid (PLA), polyethylene terephthalate, and polyurethane) through QD-based photoreforming reactions.[58] For example, the PLA plastic conversion can reach as high as 38.8 ± 4.0%, with the generation of H_2 and CO_2 as nontoxic byproducts. Later, the same group reported the feasibility of using nontoxic and inexpensive carbon nitride/nickel phosphide (CN_x|Ni_2P) as a photocatalyst for plastic reforming.[75] Although the low reaction yield and product selectivity along with the required harsh alkaline conditions largely limit the choices of QD catalysts and practical implementations, the studies promisingly demonstrate the potential of QD photocatalysts in the use of upcycling unreactive plastic waste to value-added products in a sustainable way. Given that, exploring efficient photocatalysts

https://doi.org/10.1021/acs.jpclett.1c01717
J. Phys. Chem. Lett. 2021, 12, 7180−7193

Table 3. Summary for QD-Photocatalyzed Redox Reactions[a]

entry	catalyst (ligands)	cocatalyst	solvent(s)	atmosphere	reaction type	light source	ref (year)
1	CdSe (oleate and TOP)	DCHA	various	N_2	C−C coupling	520 mW LEDs, 440−460 nm	76 (2017)
2	CdS (oleate and OPA)	none	benzene	N_2	C−C coupling	13 mW laser, 405 nm	77 (2017)
3	ZnSe-CdS (stearate, TOP, OA, and ODA)	DIPEA	hexane	N_2	C−H arylation	2.45 W LEDs, 440−470 nm	40 (2017)
4	CdS (various ligands)	none	CH_3CN	N_2	biomass valorization	300 W Xe lamp, 420−780 nm	78 and 81 (2018, 2019)
5	CdSe (oleate/phosphonate)	none	DCM	air	C−O cleavage	200 mW/cm^2, white LED	86 (2019)
6	InP−ZnS (MUA)	none	benzene	Ar	C−C coupling	1 W LED, ∼ 465 nm	79 (2019)
7	CdSe (oleate)	none	THF	N_2	intermolecular [2 + 2] cycloadditions	16.5 W LED, white light	80 (2019)
8	$APbBr_3$ (A = Cs, MA) (octylamine)	Ni	various	air	C−C, C−O coupling, *N*-heterocyclization	12 W LED, 455 nm	82 (2019)
9	$CsPbBr_3$ (oleate)	DCHA	toluene	N_2	*α*-alkylation	12 W, 400 nm	83 (2020)
10	CdSe QDs (thiolate)	none	H_2O	N_2	polymerization	5 mW laser, 532 nm	83 (2020)
11	CdSe nanoplates (oleate)	none	THF	N_2	intermolecular [2 + 2] cycloadditions	16.5 W LED, white light	85 (2021)

[a]DCHA, dicyclohexylamine; DCM, dichloromethane; MUA, 11-mercaptoundecanoic acid.

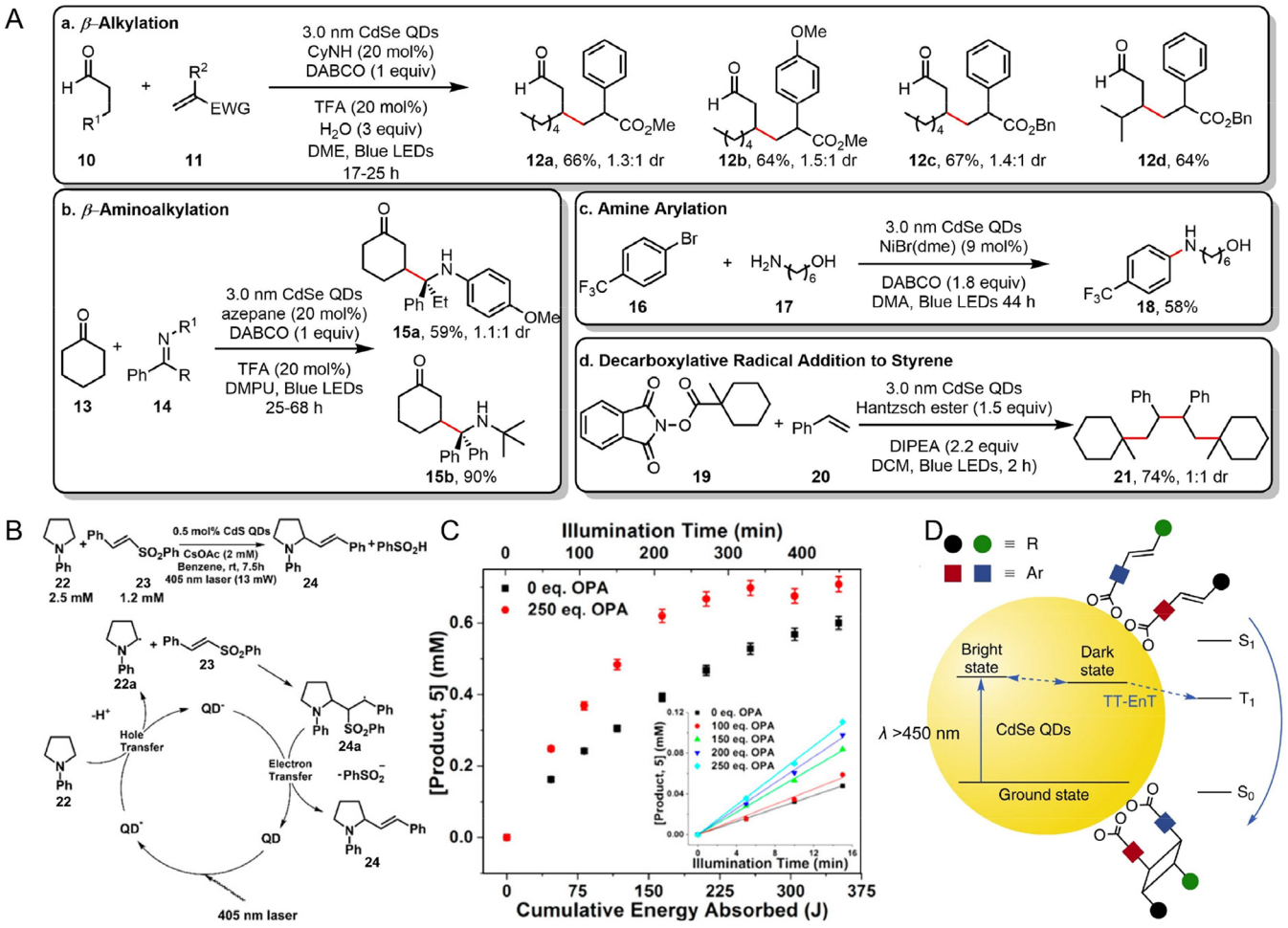

Figure 5. (A) Scope of photoredox reactions catalyzed by CdSe QDs. Reproduced from ref 76. Copyright 2017 American Chemical Society. (B) Conditions and catalytic cycle for the coupling reaction of 1-phenylpyrrolidine, **22**, and phenyl trans-styryl sulfone, **23**. (C) Concentration of product **24** vs cumulative energy absorbed and vs illumination time for the reaction in panel B, using QDs with their native oleate ligands ("0 equiv OPA") or pretreated with 250 equiv of OPA. Inset: GC-determined concentration of product **24** vs time for the first 15 min of illumination for the reaction in panel B, using QDs pretreated with different equivalents of OPA. (B and C) Reproduced from ref 77. Copyright 2017 American Chemical Society. (D) Sensitization of T_1 of the substrate through TT EnT from CdSe QDs and the *syn*-HH selectivity of CdSe QDs. Reproduced with permission from ref 80. Copyright 2019 Nature Publishing Group.

https://doi.org/10.1021/acs.jpclett.1c01717
J. Phys. Chem. Lett. 2021, 12, 7180−7193

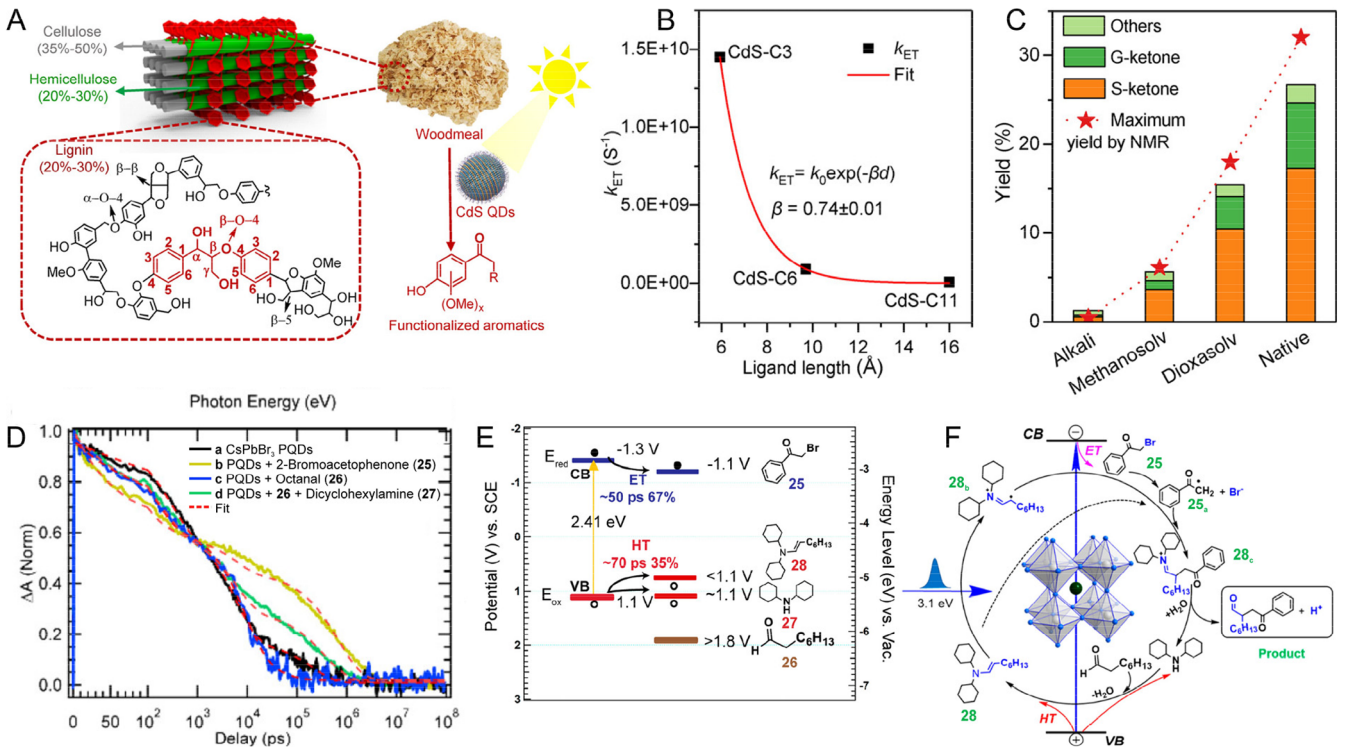

Figure 6. (A) Schematic illustration of the lignocellulose structure and photocatalytic valorization of native lignin. Major components of lignocellulosic biomass are illustrated, and the representative chemical structure of the lignin fragment is presented with the β-O-4 linkage highlighted in crimson. (B) k_{ET} vs ligand length. The value of d corresponds to the fully extended conformations of ligands. (C) Yield of aromatic monomers for photocatalytic conversion of lignins with different β-O-4 contents from different sources. (A–C) Reproduced from ref 81. Copyright 2019 American Chemical Society. (D) Normalized TA kinetics probed at the center of the perovskite QDs exciton bleach spectrum for a–d. Red-dashed traces are fits to kinetics. (E) Electrochemical potential and energy level for $CsPbBr_3$ perovskite QDs and reactants. (F) Proposed reaction mechanism for α-alkylation catalyzed by $CsPbBr_3$ perovskite QDs. (D–F) Reproduced from ref 84. Copyright 2020 American Chemical Society.

for plastic upcycling under mild conditions is still a pressing need, represeting an active but challenging research direction.

Redox Neutral Reactions. The first reports using QDs for redox neutral organic transformation were published in 2017,[76,77] which were followed by extensive studies in the past few years (Table 3).[40,76−84] In 2017, Krauss's and Weix's groups reported photoredox catalysis using CdSe QDs for versatile C−C bond formation, including β-alkylation, β-aminoalkylation, amine arylation, and decarboxylative radical addition to styrene (Figure 5A).[76] This work demonstrated that even single-sized CdSe QDs can replace the most widely used molecular photocatalysts (*i.e.*, $Ru(bpy)_3X_2$ and $Ir(ppy)_2(dtbbpy)X$) in different reactions, implying the potential of utilizing QD photocatalysts in a wide scope. At the same time, Weiss's group reported the C−C coupling reaction between 1-phenylpyrrolidine (PhPyr) and phenyl *trans*-styryl sulfone ($PhSO_2$) using colloidal CdS QDs (Figure 5B).[77] A kinetic study showed that the reaction is first-order with respect to one substrate (PhPyr) and zeroth-order with respect to the other substrate ($PhSO_2$).[77] This result indicated the rate-limiting step of the reaction was the hole transfer process from the photoexcited CdS QDs to PhPyr (Figure 5B). The authors also investigated the effect of ligand shell of CdS QDs on the reaction efficiency by partially replacing the native oleate ligands with different amount of octylphosphonic acid (OPA) ligands.[77] The shorter carbon chain without any double bond of OPA ligands can disrupt the organization of crystalline portions of the oleate shell and thus increase the permeability of small starting molecules (*i.e.*, PhPyr and $PhSO_2$) to the QD surface. The authors demonstrated that the increased permeability to QD surfaces boosted the initial reaction rate as well as the efficiency of the reaction (Figure 5C).[77] The same reaction can also be achieved using InP−ZnS core−shell QDs.[79] In addition to replacing metal complexes for photocatalytic redox neutral reactions discussed above, QDs have also been demonstrated to act as efficient catalysts for the synthesis of *syn*-tetrasubstituted cyclobutanes *via* regio- and diastereoselective intermolecular [2 + 2] cycloadditions, which are typically the side-products of metal complex-catalyzed reactions (Figure 5D).[80] In these reactions, TA spectroscopy studies demonstrated that the photocatalytic reactions were initiated by triplet−triplet energy transfer (TT EnT) instead of charge transfer from the CdSe QDs to the organic molecules (*i.e.*, 4-vinylbenzoic acid derivatives in this study). The selectivity of the kinetically disfavored *syn*-configuration can be explained by the prearrangement of the substrates at the QD surface (Figure 5D). Later, the reaction scope was expanded to conversions of internal and terminal dienes to *syn*−*trans* vinylcyclobutanes with chemo- and stereoselectivity.[85]

Beyond small organic molecule transformations, CdS QDs were successfully employed in the so-called lignin-first approach, valorizing native lignin in biomass to functionalized aromatics in the first step, with the goal of utilizing the entire lignocellulosic biomass more efficiently (Figure 6A).[78,81] In these studies, CdS QDs were demonstrated to be able to catalyze the selective cleavage of β-O-4 bonds through an electron−hole coupled oxidative dehydrogenation and sequen-

https://doi.org/10.1021/acs.jpclett.1c01717
J. Phys. Chem. Lett. 2021, 12, 7180−7193

tial reductive bond cleavage.[78,81] The authors found that the ligands of QDs played significant roles in the photocatalytic conversion of solid native lignin. First, forming a clear QD colloidal solution, which can be tuned by the hydrophilicity of ligands, was found to be mandatory for efficient lignin conversion. Second, the energy barrier for transferring charge carriers from QDs to the environment is dependent on the anchor group of the ligands. Third, for the ligands with same anchor group, the decrease of ligand length can facilitate the charge carrier transfer. Evidently, for CdS QDs capped with MPA (CdS-C3), 6-mercaptohexanoic acid (CdS-C6), and 11-mercaptoundecanoic acid (CdS-C11), the rate constant of electron transfer to 2-phenoxy-1-phenylethanol (PP-ol) can be derived from TA spectroscopic measurements (Figure 6B). The fitted rate constant showed exponential attenuation as a function of ligand length, demonstrating a ligand-mediated electron-tunneling pathway (Figure 6B).[81] The CdS-C3 QDs can further catalyze the transformation of various technical lignins, indicating a good selectivity of β-O-4 bond cleavage and a high adaptability to different substrates in the current reaction conditions.[81] Furthermore, CdSe QDs with a wider range of visible light absorption were also demonstrated as effective catalysts for cleavage of the C−O bond in a lignin model substrate, demonstrating their promise in the field of biomass depolymerization. It is noted that the CdSe QDs outperformed state-of-the-art molecular Ir-based catalysts with a greater turnover frequency.[86]

Aside from conventional QDs (*e.g.*, CdSe and CdS QDs), perovskite QDs have great potential for photoredox organic transformations because of their superior charge separation and transfer capability..[87] Yan's group demonstrated that $APbBr_3$ (A = Cs or methylammonium (MA)) perovskite QDs with a broad size distribution (2−100 nm) can be used for catalyzing a series of C−C, C−N, and C−O bond formation reactions.[82,88] Importantly, all these redox reactions are air-tolerant in contrast to inert gas-protected reactions in other catalytic systems using Cd-based QDs or molecular complexes as photocatalysts.[82,88] To understand the detailed reaction mechanism of $CsPbBr_3$ perovskite QD-photocatalyzed C−C bond formation, TA spectroscopic studies were carried out for a model reaction, *i.e.*, α-alkylation of aldehydes (substrate, 2-bromoacetophenone and octanal) (Figure 6D).[84] The initial fast decay (~50 ps) followed by a much slower decay in the microsecond time scale for **b** (QDs + 2-bromoacetophenone) and **d** (QDs + octanal + dicyclohexylamine) indicated an ultrafast charge transfer process, leading to a long-lived charge-separated state (Figure 6D). A similar decay kinetics (*i.e.*, a rapid charge transfer to a charge separated state) was observed for the system involving only perovskite QDs and cocatalyst dicyclohexylamine, while no long-lived charge-separated state was seen for **c** (QDs + octanal), indicating the charge transfer happened between the QDs and the cocatalyst (Figure 6D). Furthermore, CV measurements showed that the photoexcited electrons can be transferred to 2-bromoacetophenone while the holes can be transferred to the *in situ* formed enamine or the cocatalyst (*i.e.*, dicyclohexylamine) instead of the reactant octanal (Figure 6E). On the basis of the reaction quantum yield (~0.2%), the authors concluded that the reaction proceeded through either a biradical (solid arrow) or a one-cycle radical (dashed arrow) mechanism rather than a chain mechanism (Figure 6F).[84]

Aside from conventional QDs (*e.g.*, CdSe and CdS QDs), perovskite QDs have great potential for photoredox organic transformations because of their superior charge separation and transfer capability.

Perspective and Future Directions. The viability of utilizing QDs as functional materials has been proven in various applications through research papers, patents, and real products. The availability as well as the facile synthesis of high-quality QDs are the major competitive advantages over current molecular photocatalysts. In addition, the precise tunability of the redox potential of QD photocatalysts and their flexibility of dissolving in different solvents through ligand engineering make QDs ideal photocatalysts for a wide scope of organic reactions. Moreover, QDs possess the advantages of both homogeneous and heterogeneous photocatalysts, *i.e.*, high solubility in different solvents that enables large catalytic area and ease of removal from the reaction mixture through centrifuge or filtration, further indicating QDs' great promise in real-world industrial applications. The prospect of QDs for transforming organics has been unveiled, as are the aspects that require further investigation. In the following paragraphs, we identify the current limitations of using QD photocatalysts in organic reactions and provide our perceptions on advanced catalyst design and techniques that can help reveal the reaction mechanisms to enrich the field.

We identify the current limitations of using QD photocatalysts in organic reactions and provide our perceptions on advanced catalyst design and techniques that can help reveal the reaction mechanisms to enrich the field.

Charge separation efficiency is a key factor for utilizing photogenerated charge carriers (*i.e.*, electrons and holes) of QDs for organic transformations.[89,90] Engineering QD nanostructures is important to overcome electrostatic attraction of electron−hole pairs (excitons) and therefore achieving more efficient charge separation. In this regard, band structure engineering through a heterostructural core−shell design (*e.g.*, reverse type I, or type II band alignments) to facilitate spatial and wave function separations of electron and hole pairs has been explored extensively, mainly in gas-phase photocatalytic reactions.[91−94] Such a concept has not yet been widely applied to organic conversion reactions, which deserves more dedicated research efforts. In addition, hybrid QD-based heterostructures achieved through deposition of oxidation (*e.g.*, metal oxides for hole delocalization) or reduction cocatalysts (*e.g.*, precious metals for electron delocalization) also hold a promise in improving the reaction efficiency and selectivity, as evidenced by their roles in gas-phase reactions.[27] However, the specific functions of such hybrid composites need to be investigated specifically for organic transformations, as heterostructures may have very different redox potential and absorption profiles compared to each component. In addition,

https://doi.org/10.1021/acs.jpclett.1c01717
J. Phys. Chem. Lett. 2021, 12, 7180−7193

QD heterostructures are found to be able to enhance multiple exciton generation (MEG), a process of generating multiple excitons by a single high-energy photon.[95] We expect that MEG might be used in photocatalytic organic transformations to boost the reaction quantum efficiency and minimize/eliminate side product formation through avoiding generation of undesired radical intermediates.

Surface ligands are another important factor that determine the overall catalytic performance of QD photocatalysts. The carbon chain length, anchoring groups, and coverage density of ligands will strongly influence the stability and recyclability of QD catalysts and also the permeability and accessibility of the substrates to active catalytic sites. These desired properties often require conflicting ligand engineering strategies; hence, a deliberate balance needs to be reached when optimizing QD catalysts through ligand shell design. In comparison to the gas-phase reactions (*e.g.*, H_2 evolution or CO_2 reduction), the ligand shell of QD catalysts plays an even more important role for organic reactions. Except for the roles of maintaining the stability and accessibility of QD catalysts, ligands can have more versatile functions to facilitate organic transformations. For example, conducting ligands can serve as charge-extraction agents to improve reaction efficiency, while redox-active ligands with desired redox potential can also participate in the reaction as a catalyst.[81] It is noted that molecular catalysts with QD anchoring groups can also be attached to the QD surface. In this case, QDs serve as a photosensitizer rather than a photocatalyst. Despite the significance of ligands, studies of QD ligand effects in photocatalyzed organic reactions have been lacking, and they are worthy of being systematically explored to customize QD-based catalysts with respect to specific substrates and their conversions.[77,81] Moreover, it is worth noting that chiral molecules can give rise to chirality of the NCs and induce enantioselectivity in catalytic reactions.[96,97] Yet, there are no reports on asymmetric organic reactions catalyzed by QDs. Successful demonstrations in the cases of metal/metal oxide NC catalyzed systems show promise.[96] We anticipate research efforts will expand into this territory in the foreseeable future.

Comprehensive studies of the underlying reaction mechanisms are imperative to developing new photocatalytic systems for efficient organic transformations. Because the reactions are initiated by photoexcited charge or energy transfer to the substrates, it is crucial to understand the charge-carrier dynamics and reaction kinetics to wholly picture the reaction mechanism. In addition to conventional techniques that are commonly used to characterize QD catalysts, time-resolved *in situ* spectroscopic and microscopic tools have recently been successfully applied to elucidate the structure and active sites of catalysts under reaction conditions.[98,99] Such studies shed light on understanding the roles of QD catalysts as well as the fate of organic reactants during the transformation. Reaction mechanism studies taking advantages of advanced *in situ* characterization tools should be very welcomed. For instance, *in situ* X-ray absorption, X-ray photoelectron, and FT-IR spectroscopies can be used to monitor the oxidation states and/or coordination environments of the substrates and/or QD catalysts, while active reaction sites of the QDs can be identified and tracked using *in situ* operando TEM measurements.[100−102]

It is worth mentioning that high stability of QD photocatalysts is generally required for reaction mechanism investigations and possible industrialization. While maintaining the performances of QD photocatalysts, researchers are encouraged to continuously explore ways to further improve the QD photocatalyst stability and recyclability that are important to industrialization, including fabrication of core−shell structure, utilization of more stable ligands, anchoring QDs on stable supports (*e.g.*, silica, alumina, carbon), *etc.*

With the inspiration of seminal pioneering efforts, applying and optimizing QDs as photocatalysts in organic transformations with expanded reaction scope and improved product selectivity are expected to be progressively investigated. QDs with suitable excited-state redox potentials hold the promise to serve as alternatives to the widely applied Ru and Ir metal complex photocatalysts in a variety of organic reactions.[84] In addition, QD-based photocatalytic systems show a unique capability of regio- and diastereoselective organic transformations due to geometrical regulations during a dynamic substrate−catalyst assembly process.[55,80] Thinking further ahead, the emerging artificial intelligence (AI)-driven technology and machine learning (ML) techniques could become a fascinating tool in assisting QD-catalyzed organic reaction optimization and catalyst design.[103−105] Although such techniques are still in their infancy for photocatalysis, Amal *et al.* have already integrated photocatalysis domain knowledge with data-driven ML, demonstrating its unprecedented power in the field.[104] With exponentially increasing computing power, enriching data availability through automated syntheses/characterizations, and advancing algorithm developments, such modern computing technologies will change the traditional tedious reaction optimization process in a revolutionary way.

AUTHOR INFORMATION

Corresponding Author

Ou Chen − *Department of Chemistry, Brown University, Providence, Rhode Island 02912, United States;* orcid.org/0000-0003-0551-090X; Email: ouchen@brown.edu

Authors

Yucheng Yuan − *Department of Chemistry, Brown University, Providence, Rhode Island 02912, United States;* orcid.org/0000-0003-3935-0967

Na Jin − *Department of Chemistry, Brown University, Providence, Rhode Island 02912, United States*

Peter Saghy − *Department of Chemistry, Brown University, Providence, Rhode Island 02912, United States*

Lacie Dube − *Department of Chemistry, Brown University, Providence, Rhode Island 02912, United States*

Hua Zhu − *Department of Chemistry, Brown University, Providence, Rhode Island 02912, United States;* orcid.org/0000-0003-2733-7837

Complete contact information is available at: https://pubs.acs.org/10.1021/acs.jpclett.1c01717

Author Contributions

†Y.Y. and N.J. contributed equally to this work.

Notes

The authors declare no competing financial interest.

ACKNOWLEDGMENTS

O.C. acknowledges the support from the National Science Foundation (DMR-1943930, CBET-1936223, and CMMI-

1934314). O.C. also acknowledges the support from the Camille & Henry Dreyfus Foundation through the Camille Dreyfus Teacher-Scholar Awards program, the Alfred P. Sloan Foundation through Sloan Research Fellowship Award program, and the 3M Foundation through the Non-Tenured Faculty Award program. P.S. is supported by Brown University through the Chancellor Robert Fellowship program. L.D. is supported by the Brown University IMSD fellowship program through NIGMS (R25GM083270).

REFERENCES

(1) Prier, C. K.; Rankic, D. A.; MacMillan, D. W. C. Visible Light Photoredox Catalysis with Transition Metal Complexes: Applications in Organic Synthesis. *Chem. Rev.* **2013**, *113*, 5322−5363.
(2) Skubi, K. L.; Blum, T. R.; Yoon, T. P. Dual Catalysis Strategies in Photochemical Synthesis. *Chem. Rev.* **2016**, *116*, 10035−10074.
(3) Cheng, W.-M.; Shang, R. Transition Metal-Catalyzed Organic Reactions under Visible Light: Recent Developments and Future Perspectives. *ACS Catal.* **2020**, *10*, 9170−9196.
(4) White, J. L.; Baruch, M. F.; Pander, J. E.; Hu, Y.; Fortmeyer, I. C.; Park, J. E.; Zhang, T.; Liao, K.; Gu, J.; Yan, Y.; et al. Light-Driven Heterogeneous Reduction of Carbon Dioxide: Photocatalysts and Photoelectrodes. *Chem. Rev.* **2015**, *115*, 12888−12935.
(5) Banerjee, T.; Gottschling, K.; Savasci, G.; Ochsenfeld, C.; Lotsch, B. V. H_2 Evolution with Covalent Organic Framework Photocatalysts. *ACS Energy Lett.* **2018**, *3*, 400−409.
(6) Wang, L.; Fan, H.; Bai, F. Porphyrin-Based Photocatalysts for Hydrogen Production. *MRS Bull.* **2020**, *45*, 49−56.
(7) Nag, A.; Kovalenko, M. V.; Lee, J. S.; Liu, W. Y.; Spokoyny, B.; Talapin, D. V. Metal-free Inorganic Ligands for Colloidal Nanocrystals: S^{2-}, HS^{-}, Se^{2-}, HSe^{-}, Te^{2-}, HTe^{-}, TeS_3^{2-}, OH^{-}, and NH^{2-} as Surface Ligands. *J. Am. Chem. Soc.* **2011**, *133*, 10612−10620.
(8) Weiss, E. A. Designing the Surfaces of Semiconductor Quantum Dots for Colloidal Photocatalysis. *ACS Energy Lett.* **2017**, *2*, 1005−1013.
(9) Kodaimati, M. S.; McClelland, K. P.; He, C.; Lian, S.; Jiang, Y.; Zhang, Z.; Weiss, E. A. Viewpoint: Challenges in Colloidal Photocatalysis and Some Strategies for Addressing Them. *Inorg. Chem.* **2018**, *57*, 3659−3670.
(10) Luo, J.; Zhang, S.; Sun, M.; Yang, L.; Luo, S.; Crittenden, J. C. A Critical Review on Energy Conversion and Environmental Remediation of Photocatalysts with Remodeling Crystal Lattice, Surface, and Interface. *ACS Nano* **2019**, *13*, 9811−9840.
(11) Chen, O.; Zhao, J.; Chauhan, V. P.; Cui, J.; Wong, C.; Harris, D. K.; Wei, H.; Han, H.-S.; Fukumura, D.; Jain, R. K.; Bawendi, M. G. Compact High-Quality CdSe−CdS Core−Shell Nanocrystals with Narrow Emission Linewidths and Suppressed Blinking. *Nat. Mater.* **2013**, *12*, 445−451.
(12) Tan, R.; Yuan, Y.; Nagaoka, Y.; Eggert, D.; Wang, X.; Thota, S.; Guo, P.; Yang, H.; Zhao, J.; Chen, O. Monodisperse Hexagonal Pyramidal and Bipyramidal Wurtzite CdSe-CdS Core−Shell Nanocrystals. *Chem. Mater.* **2017**, *29*, 4097−4108.
(13) Zhu, H.; Cai, T.; Que, M.; Song, J.-P.; Rubenstein, B. M.; Wang, Z.; Chen, O. Pressure-Induced Phase Transformation and Band-Gap Engineering of Formamidinium Lead Iodide Perovskite Nanocrystals. *J. Phys. Chem. Lett.* **2018**, *9*, 4199−4205.
(14) Cai, T.; Yang, H.; Hills-Kimball, K.; Song, J.-P.; Zhu, H.; Hofman, E.; Zheng, W.; Rubenstein, B. M.; Chen, O. Synthesis of All-Inorganic Cd-Doped $CsPbCl_3$ Perovskite Nanocrystals with Dual-Wavelength Emission. *J. Phys. Chem. Lett.* **2018**, *9*, 7079−7084.
(15) Luo, Y.; Wang, Y. C.; Liu, M. Q.; Zhu, H.; Chen, O.; Zou, S. L.; Zhao, J. Colloidal Assembly of Au-Quantum Dot-Au Sandwiched Nanostructures with Strong Plasmon-Exciton Coupling. *J. Phys. Chem. Lett.* **2020**, *11*, 2449−2456.
(16) Liu, Z.; Yang, H.; Wang, J.; Yuan, Y.; Hills-Kimball, K.; Cai, T.; Wang, P.; Tang, A.; Chen, O. Synthesis of Lead-Free Cs_2AgBiX_6 (X = Cl, Br, I) Double Perovskite Nanoplatelets and Their Application in CO_2 Photocatalytic Reduction. *Nano Lett.* **2021**, *21*, 1620−1627.
(17) Chen, B. K.; Pradhan, N.; Zhong, H. From Large-Scale Synthesis to Lighting Device Applications of Ternary I-III-VI Semiconductor Nanocrystals: Inspiring Greener Material Emitters. *J. Phys. Chem. Lett.* **2018**, *9*, 435−445.
(18) Li, B.; Zhang, G.; Zhang, Y.; Yang, C.; Guo, W.; Peng, Y.; Chen, R.; Qin, C.; Gao, Y.; Hu, J.; et al. Biexciton Dynamics in Single Colloidal CdSe Quantum Dots. *J. Phys. Chem. Lett.* **2020**, *11*, 10425−10432.
(19) Hendricks, M. P.; Campos, M. P.; Cleveland, G. T.; Jen-La Plante, I.; Owen, J. S. A Tunable Library of Substituted Thiourea Precursors to Metal Sulfide Nanocrystals. *Science* **2015**, *348*, 1226−1230.
(20) Zhou, J.; Xia, Z.; Molokeev, M. S.; Zhang, X.; Peng, D.; Liu, Q. Composition Design, Optical Gap and Stability Investigations of Lead-Free Halide Double Perovskite $Cs_2AgInCl_6$. *J. Mater. Chem. A* **2017**, *5*, 15031−15037.
(21) Gao, F.; Wu, J.; Zhao, Y.; Song, T.; Deng, Z.; Wang, P.; Wang, Y.; Li, H. A General Approach to Realizing Perovskite Nanocrystals with Insulating Metal Sulfate Shells. *Nanoscale* **2021**, *13*, 10329−10334.
(22) Luo, Z.; Li, Q.; Zhang, L.; Wu, X.; Tan, L.; Zou, C.; Liu, Y.; Quan, Z. 0D $Cs_3Cu_2X_5$ (X = I, Br, and Cl) Nanocrystals: Colloidal Syntheses and Optical Properties. *Small* **2020**, *16*, 1905226.
(23) Roberge, A.; Stein, J. L.; Shen, Y.; Cossairt, B. M.; Greytak, A. B. Purification and In Situ Ligand Exchange of Metal-Carboxylate-Treated Fluorescent InP Quantum Dots via Gel Permeation Chromatography. *J. Phys. Chem. Lett.* **2017**, *8*, 4055−4060.
(24) Nie, Y.-C.; Yu, F.; Wang, L.-C.; Xing, Q.-J.; Liu, X.; Pei, Y.; Zou, J.-P.; Dai, W.-L.; Li, Y.; Suib, S. L. Photocatalytic Degradation of Organic Pollutants Coupled with Simultaneous Photocatalytic H_2 Evolution over Graphene Quantum Dots/Mn-N-TiO_2/g-C_3N_4 Composite Catalysts: Performance and Mechanism. *Appl. Catal., B* **2018**, *227*, 312−321.
(25) Kampouri, S.; Stylianou, K. C. Dual-Functional Photocatalysis for Simultaneous Hydrogen Production and Oxidation of Organic Substances. *ACS Catal.* **2019**, *9* (5), 4247−4270.
(26) Li, J.-Y.; Li, Y.-H.; Qi, M.-Y.; Lin, Q.; Tang, Z.-R.; Xu, Y.-J. Selective Organic Transformations over Cadmium Sulfide-Based Photocatalysts. *ACS Catal.* **2020**, *10*, 6262−6280.
(27) Lu, H.; Huang, Z.; Martinez, M. S.; Johnson, J. C.; Luther, J. M.; Beard, M. C. Transforming Energy Using Quantum Dots. *Energy Environ. Sci.* **2020**, *13*, 1347−1376.
(28) Yanagida, S.; Azuma, T.; Midori, Y.; Pac, C.; Sakurai, H. Semiconductor Photocatalysis. Part 4. Hydrogen Evolution and Photoredox Reactions of Cyclic Ethers Catalysed by Zinc Sulphide. *J. Chem. Soc., Perkin Trans. 2* **1985**, 1487−1493.
(29) Yanagida, S.; Kizumoto, H.; Ishimaru, Y.; Pac, C.; Sakurai, H. Zinc Sulfide-Catalyzed Photochemical Conversion of Primary Amines to Secondary Amines. *Chem. Lett.* **1985**, *14*, 141−144.
(30) Yanagida, S.; Yoshiya, M.; Shiragami, T.; Pac, C.; Mori, H.; Fujita, H. Semiconductor Photocatalysis. I. Quantitative Photoreduction of Aliphatic Ketones to Alcohols Using Defect-Free Zinc Sulfide Quantum Crystallites. *J. Phys. Chem.* **1990**, *94*, 3104−3111.
(31) Shiragami, T.; Ankyu, H.; Fukami, S.; Pac, C.; Yanaglda, S.; Mori, H.; Fujita, H. Semiconductor Photocatalysis: Visible Light Induced Photoreduction of Aromatic Ketones and Electron-Deficient Alkenes Catalysed by Quantised Cadmium Sulfide. *J. Chem. Soc., Faraday Trans.* **1992**, *88*, 1055−1061.
(32) Yanagida, S.; Ogata, T.; Shindo, A.; Hosokawa, H.; Mori, H.; Sakata, T.; Wada, Y. Semiconductor Photocatalysis: Size Control of Surface-Capped CdS Nanocrystallites and the Quantum Size Effect in Their Photocatalysis. *Bull. Chem. Soc. Jpn.* **1995**, *68*, 752−758.
(33) Hosokawa, H.; Ogata, T.; Wada, Y.; Murakoshi, K.; Sakata, T.; Mori, H.; Yanagida, S. Surface Modification of CdS Quantum Dots with Fluorinated Thiophenol. *J. Chem. Soc., Faraday Trans.* **1996**, *92*, 4575−4580.
(34) Torimoto, T.; Uchida, H.; Sakata, T.; Mori, H.; Yoneyama, H. Surface Structures of Lead Sulfide Microcrystals Modified with 4-

https://doi.org/10.1021/acs.jpclett.1c01717
J. Phys. Chem. Lett. 2021, 12, 7180−7193

(Hydroxythio)phenol and Their Influences on Photoinduced Charge Transfer. *J. Am. Chem. Soc.* **1993**, *115*, 1874−1880.
(35) Torimoto, T.; Sakata, T.; Mori, H.; Yoneyama, H. Effect of Surface Charge of 4-Aminothiophenol-Modified PbS Microcrystal Photocatalysts on Photoinduced Charge Transfer. *J. Phys. Chem.* **1994**, *98*, 3036−3043.
(36) Inoue, H.; Ichiroku, N.; Torimoto, T.; Sakata, T.; Mori, H.; Yoneyama, H. Photoinduced Electron Transfer from Zinc Sulfide Microcrystals Modified with Various Alkanethiols to Methyl Viologen. *Langmuir* **1994**, *10*, 4517−4522.
(37) Torimoto, T.; Maeda, K.; Maenaka, J.; Yoneyama, H. Photoelectrochemical Properties of Size-Quantized CdS Microcrystals Modified with Various Amounts of Viologen-Functionalized Thiol. *J. Phys. Chem.* **1994**, *98*, 13658−13664.
(38) Wada, Y.; Kitamura, T.; Yanagida, S.; Yin, H. Photoreductive Dechlorination of Chlorinated Benzene Derivatives Catalyzed by ZnS Nanocrystallites. *Chem. Commun.* **1998**, 2683−2684.
(39) Yin, H.; Wada, Y.; Kitamura, T.; Yanagida, S. Photoreductive Dehalogenation of Halogenated Benzene Derivatives Using ZnS or CdS Nanocrystallites as Photocatalysts. *Environ. Sci. Technol.* **2001**, *35*, 227−231.
(40) Pal, A.; Ghosh, I.; Sapra, S.; König, B. Quantum Dots in Visible-Light Photoredox Catalysis: Reductive Dehalogenations and C−H Arylation Reactions Using Aryl Bromides. *Chem. Mater.* **2017**, *29*, 5225−5231.
(41) Warrier, M.; Lo, M. K. F.; Monbouquette, H.; Garcia-Garibay, M. A. Photocatalytic Reduction of Aromatic Azides to Amines Using CdS and CdSe Nanoparticles. *Photochem. Photobiol. Sci.* **2004**, *3*, 859−863.
(42) Pal, B.; Torimoto, T.; Okazaki, K. I.; Ohtani, B. Photocatalytic Syntheses of Azoxybenzene by Visible Light Irradiation of Silica-Coated Cadmium Sulfide Nanocomposites. *Chem. Commun.* **2007**, 483−485.
(43) Eskandari, P.; Kazemi, F.; Zand, Z. Photocatalytic Reduction of Aromatic Nitro Compounds Using CdS Nanostructure under Blue LED Irradiation. *J. Photochem. Photobiol., A* **2014**, *274*, 7−12.
(44) Jensen, S. C.; Bettis Homan, S.; Weiss, E. A. Photocatalytic Conversion of Nitrobenzene to Aniline through Sequential Proton-Coupled One-Electron Transfers from a Cadmium Sulfide Quantum Dot. *J. Am. Chem. Soc.* **2016**, *138*, 1591−1600.
(45) Huang, Y.; Zhu, Y.; Egap, E. Semiconductor Quantum Dots as Photocatalysts for Controlled Light-Mediated Radical Polymerization. *ACS Macro Lett.* **2018**, *7*, 184−189.
(46) Xi, Z.-W.; Yang, L.; Wang, D.-Y.; Pu, C.-D.; Shen, Y.-M.; Wu, C.-D.; Peng, X.-G. Visible-Light Photocatalytic Synthesis of Amines from Imines via Transfer Hydrogenation Using Quantum Dots as Catalysts. *J. Org. Chem.* **2018**, *83*, 11886−11895.
(47) Hu, J.; Pu, T.-J.; Xu, Z.-W.; Xu, W.-Y.; Feng, Y.-S. Cadmium Sulfide Quantum-Dot-Photocatalyzed Cascade Cyclization of Functionalized Difluoromethyl Chlorides with Unactivated Olefins. *Adv. Synth. Catal.* **2019**, *361*, 708−713.
(48) Perez, K. A.; Rogers, C. R.; Weiss, E. A. Quantum Dot-Catalyzed Photoreductive Removal of Sulfonyl-Based Protecting Groups. *Angew. Chem., Int. Ed.* **2020**, *59*, 14091−14095.
(49) Tafesh, A. M.; Weiguny, J. A Review of the Selective Catalytic Reduction of Aromatic Nitro Compounds into Aromatic Amines, Isocyanates, Carbamates, and Ureas Using CO. *Chem. Rev.* **1996**, *96*, 2035−2052.
(50) Yu, C.; Liu, B.; Hu, L. Samarium(0) and 1,1′-Dioctyl-4,4′-Bipyridinium Dibromide: A Novel Electron-Transfer System for the Chemoselective Reduction of Aromatic Nitro Groups. *J. Org. Chem.* **2001**, *66*, 919−924.
(51) Li, Y.-P.; Cao, H.-B.; Liu, C.-M.; Zhang, Y. Electrochemical Reduction of Nitrobenzene at Carbon Nanotube Electrode. *J. Hazard. Mater.* **2007**, *148*, 158−163.
(52) Li, Z. J.; Li, S. Y.; Davis, A. H.; Hofman, E.; Leem, G.; Zheng, W. W. Enhanced Singlet Oxygen Generation by Hybrid Mn-Doped Nanocomposites for Selective Photo-Oxidation of Benzylic Alcohols. *Nano Res.* **2020**, *13*, 1668−1676.
(53) Mahdavi-Shakib, A.; Sempel, J.; Hoffman, M.; Oza, A.; Bennett, E.; Owen, J. S.; Rahmani Chokanlu, A.; Frederick, B. G.; Austin, R. N. Au/TiO_2-Catalyzed Benzyl Alcohol Oxidation on Morphologically Precise Anatase Nanoparticles. *ACS Appl. Mater. Interfaces* **2021**, *13*, 11793−11804.
(54) Bernt, C. M.; Burks, P. T.; DeMartino, A. W.; Pierri, A. E.; Levy, E. S.; Zigler, D. F.; Ford, P. C. Photocatalytic Carbon Disulfide Production via Charge Transfer Quenching of Quantum Dots. *J. Am. Chem. Soc.* **2014**, *136*, 2192−2195.
(55) Yuan, Y.; Zhu, H.; Hills-Kimball, K.; Cai, T.; Shi, W.; Wei, Z.; Yang, H.; Candler, Y.; Wang, P.; He, J.; Chen, O. Stereoselective C−C Oxidative Coupling Reactions Photocatalyzed by Zwitterionic Ligand Capped $CsPbBr_3$ Perovskite Quantum Dots. *Angew. Chem., Int. Ed.* **2020**, *59*, 22563−22569.
(56) Huang, C.; Li, X.-B.; Tung, C.-H.; Wu, L.-Z. Photocatalysis with Quantum Dots and Visible Light for Effective Organic Synthesis. *Chem. - Eur. J.* **2018**, *24*, 11530−11534.
(57) Hao, H.; Lang, X. Metal Sulfide Photocatalysis: Visible-Light-Induced Organic Transformations. *ChemCatChem* **2019**, *11*, 1378−1393.
(58) Uekert, T.; Kuehnel, M. F.; Wakerley, D. W.; Reisner, E. Plastic Waste as A Feedstock for Solar-Driven H_2 Generation. *Energy Environ. Sci.* **2018**, *11*, 2853−2857.
(59) Yurdakal, S.; Palmisano, G.; Loddo, V.; Augugliaro, V.; Palmisano, L. Nanostructured Rutile TiO_2 for Selective Photocatalytic Oxidation of Aromatic Alcohols to Aldehydes in Water. *J. Am. Chem. Soc.* **2008**, *130*, 1568−1569.
(60) Zhao, L. M.; Meng, Q. Y.; Fan, X. B.; Ye, C.; Li, X. B.; Chen, B.; Ramamurthy, V.; Tung, C. H.; Wu, L. Z. Photocatalysis with Quantum Dots and Visible Light: Selective and Efficient Oxidation of Alcohols to Carbonyl Compounds through a Radical Relay Process in Water. *Angew. Chem., Int. Ed.* **2017**, *56*, 3020−3024.
(61) McClelland, K. P.; Weiss, E. A. Selective Photocatalytic Oxidation of Benzyl Alcohol to Benzaldehyde or C-C Coupled Products by Visible-Light-Absorbing Quantum Dots. *ACS Appl. Energy Mater.* **2019**, *2*, 92−96.
(62) Tamiolakis, I.; Lykakis, I. N.; Armatas, G. S. Mesoporous CdS-Sensitized TiO_2 Nanoparticle Assemblies with Enhanced Photocatalytic Properties: Selective Aerobic Oxidation of Benzyl Alcohols. *Catal. Today* **2015**, *250*, 180−186.
(63) Huang, M. H.; Dai, X. C.; Li, T.; Li, Y. B.; He, Y. H.; Xiao, G. C.; Xiao, F. X. Stimulating Charge Transfer Over Quantum Dots via Ligand-Triggered Layer-by-Layer Assembly toward Multifarious Photoredox Organic Transformation. *J. Phys. Chem. C* **2019**, *123*, 9721−9734.
(64) Wang, J. G.; Liang, H.; Zhang, C.; Jin, B.; Men, Y. Bi_2WO_{6-x} Nanosheets with Tunable Bi Quantum Dots and Oxygen Vacancies for Photocatalytic Selective Oxidation of Alcohols. *Appl. Catal., B* **2019**, *256*, 117874.
(65) Chen, K.; Deng, X.; Dodekatos, G.; Tüysüz, H. Photocatalytic Polymerization of 3,4-Ethylenedioxythiophene over Cesium Lead Iodide Perovskite Quantum Dots. *J. Am. Chem. Soc.* **2017**, *139*, 12267−12273.
(66) Chauvire, T.; Mouesca, J. M.; Gasparutto, D.; Ravanat, J. L.; Lebrun, C.; Gromova, M.; Jouneau, P. H.; Chauvin, J.; Gambarelli, S.; Maurel, V. Redox Photocatalysis with Water-Soluble Core Shell CdSe-ZnS Quantum Dots. *J. Phys. Chem. C* **2015**, *119*, 17857−17866.
(67) Zhang, J. H.; Liu, J. C.; Wang, X. Y.; Mai, J. J.; Zhao, W.; Ding, Z. X.; Fang, Y. X. Construction of Z-Scheme Tungsten Trioxide Nanosheets-Nitrogen-Doped Carbon Dots Composites for the Enhanced Photothermal Synergistic Catalytic Oxidation of Cyclohexane. *Appl. Catal., B* **2019**, *259*, 118063.
(68) Mahmood, A.; Wang, X.; Shi, G.; Wang, Z.; Xie, X.; Sun, J. Revealing Adsorption and the Photodegradation Mechanism of Gas Phase *o*-xylene on Carbon Quantum Dots Modified TiO_2 Nanoparticles. *J. Hazard. Mater.* **2020**, *386*, 121962.
(69) Li, H. T.; Sun, C. H.; Ali, M. T.; Zhou, F. L.; Zhang, X. Y.; MacFarlane, D. R. Sulfated Carbon Quantum Dots as Efficient

https://doi.org/10.1021/acs.jpclett.1c01717
J. Phys. Chem. Lett. 2021, 12, 7180−7193

Visible-Light Switchable Acid Catalysts for Room-Temperature Ring-Opening Reactions. *Angew. Chem., Int. Ed.* **2015**, *54*, 8420−8424.
(70) Li, X. B.; Li, Z. J.; Gao, Y. J.; Meng, Q. Y.; Yu, S.; Weiss, R. G.; Tung, C. H.; Wu, L. Z. Mechanistic Insights into the Interface-Directed Transformation of Thiols into Disulfides and Molecular Hydrogen by Visible-Light Irradiation of Quantum Dots. *Angew. Chem., Int. Ed.* **2014**, *53*, 2085−2089.
(71) Suzuki, A. Cross-Coupling Reactions Of Organoboranes: An Easy Way To Construct C-C Bonds (Nobel Lecture). *Angew. Chem., Int. Ed.* **2011**, *50*, 6722−6737.
(72) Zou, J. P.; Wu, D. D.; Luo, J. M.; Xing, Q. J.; Luo, X. B.; Dong, W. H.; Luo, S. L.; Du, H. M.; Suib, S. L. A Strategy for One-Pot Conversion of Organic Pollutants into Useful Hydrocarbons through Coupling Photodegradation of MB with Photoreduction of CO_2. *ACS Catal.* **2016**, *6*, 6861−6867.
(73) Mou, Z. G.; Zhang, H.; Liu, Z. M.; Sun, J. H.; Zhu, M. S. Ultrathin BiOCl/Nitrogen-Doped Graphene Quantum Dots Composites with Strong Adsorption and Effective Photocatalytic Activity for the Degradation of Antibiotic Ciprofloxacin. *Appl. Surf. Sci.* **2019**, *496*, 143655.
(74) Malankowska, A.; Kulesza, D.; Sowik, J.; Cavdar, O.; Klimczuk, T.; Trykowski, G.; Zaleska-Medynska, A. The Effect of $AgInS_2$, SnS, CuS_2, Bi_2S_3 Quantum Dots on the Surface Properties and Photocatalytic Activity of QDs-Sensitized TiO_2 Composite. *Catalysts* **2020**, *10*, 403.
(75) Uekert, T.; Kasap, H.; Reisner, E. Photoreforming of Nonrecyclable Plastic Waste over a Carbon Nitride/Nickel Phosphide Catalyst. *J. Am. Chem. Soc.* **2019**, *141* (38), 15201−15210.
(76) Caputo, J. A.; Frenette, L. C.; Zhao, N.; Sowers, K. L.; Krauss, T. D.; Weix, D. J. General and Efficient C−C Bond Forming Photoredox Catalysis with Semiconductor Quantum Dots. *J. Am. Chem. Soc.* **2017**, *139*, 4250−4253.
(77) Zhang, Z.; Edme, K.; Lian, S.; Weiss, E. A. Enhancing the Rate of Quantum-Dot-Photocatalyzed Carbon−Carbon Coupling by Tuning the Composition of the Dot's Ligand Shell. *J. Am. Chem. Soc.* **2017**, *139*, 4246−4249.
(78) Wu, X.; Fan, X.; Xie, S.; Lin, J.; Cheng, J.; Zhang, Q.; Chen, L.; Wang, Y. Solar Energy- Driven Lignin-First Approach to Full Utilization of Lignocellulosic Biomass under Mild Conditions. *Nat. Catal.* **2018**, *1*, 772−780.
(79) Chakraborty, I. N.; Roy, S.; Devatha, G.; Rao, A.; Pillai, P. P. InP/ZnS Quantum Dots as Efficient Visible-Light Photocatalysts for Redox and Carbon−Carbon Coupling Reactions. *Chem. Mater.* **2019**, *31*, 2258−2262.
(80) Jiang, Y.; Wang, C.; Rogers, C. R.; Kodaimati, M. S.; Weiss, E. A. Regio- and Diastereoselective Intermolecular [2 + 2] Cycloadditions Photocatalysed by Quantum Dots. *Nat. Chem.* **2019**, *11*, 1034−1040.
(81) Wu, X.; Xie, S.; Liu, C.; Zhou, C.; Lin, J.; Kang, J.; Zhang, Q.; Wang, Z.; Wang, Y. Ligand-Controlled Photocatalysis of CdS Quantum Dots for Lignin Valorization under Visible Light. *ACS Catal.* **2019**, *9*, 8443−8451.
(82) Zhu, X.; Lin, Y.; San Martin, J.; Sun, Y.; Zhu, D.; Yan, Y. Lead Halide Perovskites for Photocatalytic Organic Synthesis. *Nat. Commun.* **2019**, *10*, 2843.
(83) McClelland, K. P.; Clemons, T. D.; Stupp, S. I.; Weiss, E. A. Semiconductor Quantum Dots Are Efficient and Recyclable Photocatalysts for Aqueous PET-RAFT Polymerization. *ACS Macro Lett.* **2020**, *9*, 7−13.
(84) Wang, K.; Lu, H.; Zhu, X.; Lin, Y.; Beard, M. C.; Yan, Y.; Chen, X. Ultrafast Reaction Mechanisms in Perovskite Based Photocatalytic C−C Coupling. *ACS Energy Lett.* **2020**, *5*, 566−571.
(85) Jiang, Y.; Yang, M.; Wu, Y.; López-Arteaga, R.; Rogers, C. R.; Weiss, E. A. Chemo- and Stereoselective Intermolecular [2 + 2] Photocycloaddition of Conjugated Dienes Using Colloidal Nanocrystal Photocatalysts. *Chem. Catal.* **2021**, *1*, 106−116.
(86) Enright, M. J.; Gilbert-Bass, K.; Sarsito, H.; Cossairt, B. M. Photolytic C-O Bond Cleavage with Quantum Dots. *Chem. Mater.* **2019**, *31*, 2677−2682.
(87) Dong, Q.; Fang, Y.; Shao, Y.; Mulligan, P.; Qiu, J.; Cao, L.; Huang, J. Electron-Hole Diffusion Lengths > 175 μm in Solution-Grown $CH_3NH_3PbI_3$ Single Crystals. *Science* **2015**, *347*, 967−970.
(88) Zhu, X.; Lin, Y.; Sun, Y.; Beard, M. C.; Yan, Y. Lead-Halide Perovskites for Photocatalytic α-Alkylation of Aldehydes. *J. Am. Chem. Soc.* **2019**, *141*, 733−738.
(89) Busby, E.; Thibert, A.; Page, L. E.; Jawaid, A. M.; Snee, P. T.; Larsen, D. S. Primary Charge Carrier Dynamics of Water-Solubilized CdZnS/ZnS Core/Shell and CdZnS/ZnS·Pd Nanoparticle Adducts. *Chem. Phys. Lett.* **2013**, *573*, 56−62.
(90) Goswami, T.; Yadav, D. K.; Bhatt, H.; Kaur, G.; Shukla, A.; Babu, K. J.; Ghosh, H. N. Defect-Mediated Slow Carrier Recombination and Broad Photoluminescence in Non-Metal-Doped $ZnIn_2S_4$ Nanosheets for Enhanced Photocatalytic Activity. *J. Phys. Chem. Lett.* **2021**, *12*, 5000−5008.
(91) Acharya, K. P.; Khnayzer, R. S.; O'Connor, T.; Diederich, G.; Kirsanova, M.; Klinkova, A.; Roth, D.; Kinder, E.; Imboden, M.; Zamkov, M. The Role of Hole Localization in Sacrificial Hydrogen Production by Semiconductor-Metal Heterostructured Nanocrystals. *Nano Lett.* **2011**, *11*, 2919−2926.
(92) Khon, E.; Lambright, K.; Khnayzer, R. S.; Moroz, P.; Perera, D.; Butaeva, E.; Lambright, S.; Castellano, F. N.; Zamkov, M. Improving the Catalytic Activity of Semiconductor Nanocrystals through Selective Domain Etching. *Nano Lett.* **2013**, *13*, 2016−2023.
(93) Wang, P.; Wang, M.; Zhang, J.; Li, C.; Xu, X.; Jin, Y. Shell Thickness Engineering Significantly Boosts the Photocatalytic H_2 Evolution Efficiency of CdS/CdSe Core/Shell Quantum Dots. *ACS Appl. Mater. Interfaces* **2017**, *9*, 35712−35720.
(94) Wu, H.-L.; Li, X.-B.; Tung, C.-H.; Wu, L.-Z. Semiconductor Quantum Dots: An Emerging Candidate for CO_2 Photoreduction. *Adv. Mater.* **2019**, *31*, 1900709.
(95) Kroupa, D. M.; Pach, G. F.; Vörös, M.; Giberti, F.; Chernomordik, B. D.; Crisp, R. W.; Nozik, A. J.; Johnson, J. C.; Singh, R.; Klimov, V. I.; Galli, G.; Beard, M. C. Enhanced Multiple Exciton Generation in PbS|CdS Janus-like Heterostructured Nanocrystals. *ACS Nano* **2018**, *12*, 10084−10094.
(96) Yasukawa, T.; Miyamura, H.; Kobayashi, S. Chiral Metal Nanoparticle-Catalyzed Asymmetric C-C Bond Formation Reactions. *Chem. Soc. Rev.* **2014**, *43*, 1450−1461.
(97) Ma, W.; Xu, L.; de Moura, A. F.; Wu, X.; Kuang, H.; Xu, C.; Kotov, N. A. Chiral Inorganic Nanostructures. *Chem. Rev.* **2017**, *117*, 8041−8093.
(98) Godin, R.; Wang, Y.; Zwijnenburg, M. A.; Tang, J. W.; Durrant, J. R. Time-Resolved Spectroscopic Investigation of Charge Trapping in Carbon Nitrides Photocatalysts for Hydrogen Generation. *J. Am. Chem. Soc.* **2017**, *139*, 5216−5224.
(99) Hu, Y. G.; Zhan, F.; Wang, Q.; Sun, Y. J.; Yu, C.; Zhao, X.; Wang, H.; Long, R.; Zhang, G. Z.; Gao, C.; Zhang, W. K.; Jiang, J.; Tao, Y.; Xiong, Y. J. Tracking Mechanistic Pathway of Photocatalytic CO_2 Reaction at Ni Sites Using Operando, Time-Resolved Spectroscopy. *J. Am. Chem. Soc.* **2020**, *142*, 5618−5626.
(100) Hülsey, M. J.; Zhang, B.; Ma, Z.; Asakura, H.; Do, D. A.; Chen, W.; Tanaka, T.; Zhang, P.; Wu, Z.; Yan, N. In situ Spectroscopy-Guided Engineering of Rhodium Single-Atom Catalysts for CO Oxidation. *Nat. Commun.* **2019**, *10*, 1330.
(101) Wu, Y. A.; McNulty, I.; Liu, C.; Lau, K. C.; Liu, Q.; Paulikas, A. P.; Sun, C. J.; Cai, Z.; Guest, J. R.; Ren, Y.; Stamenkovic, V.; Curtiss, L. A.; Liu, Y.; Rajh, T. Facet-Dependent Active Sites of A Single Cu_2O Particle Photocatalyst for CO_2 Reduction to Methanol. *Nat. Energy* **2019**, *4*, 957−968.
(102) Yin, Z.-W.; Betzler, S. B.; Sheng, T.; Zhang, Q.; Peng, X.; Shangguan, J.; Bustillo, K. C.; Li, J.-T.; Sun, S.-G.; Zheng, H. Visualization of Facet-Dependent pseudo-Photocatalytic Behavior of TiO_2 Nanorods for Water Splitting Using In situ Liquid Cell TEM. *Nano Energy* **2019**, *62*, 507−512.
(103) Empel, C.; Koenigs, R. M. Artificial-Intelligence-Driven Organic Synthesis—En Route towards Autonomous Synthesis? *Angew. Chem., Int. Ed.* **2019**, *58*, 17114−17116.

https://doi.org/10.1021/acs.jpclett.1c01717
J. Phys. Chem. Lett. 2021, 12, 7180−7193

(104) Masood, H.; Toe, C. Y.; Teoh, W. Y.; Sethu, V.; Amal, R. Machine Learning for Accelerated Discovery of Solar Photocatalysts. *ACS Catal.* **2019**, *9*, 11774−11787.
(105) Toyao, T.; Maeno, Z.; Takakusagi, S.; Kamachi, T.; Takigawa, I.; Shimizu, K. I. Machine Learning for Catalysis Informatics: Recent Applications and Prospects. *ACS Catal.* **2020**, *10*, 2260−2297.

https://doi.org/10.1021/acs.jpclett.1c01717
J. Phys. Chem. Lett. 2021, 12, 7180−7193